# State-of-charge estimation of lithium-ion battery based on second order resistor-capacitance circuit-PSO-TCN model

Feng Li[a] Wei Zuo[a, e*] Kun Zhou[a,e] Qingqing Li[a, e] Yuhan Huang[b, c] Guangde Zhang[d]

*a. The State Key Laboratory of Refractories and Metallurgy, Wuhan University of Science and Technology, Wuhan 430081, China*

*b. Centre for Green Technology, School of Civil and Environmental Engineering, University of Technology Sydney, NSW 2007, Australia*

*c. Department of Engineering Science, University of Oxford, Oxford OX1 3PJ, United Kingdom*

*d. School of Automobile and Traffic Engineering, Wuhan University of Science and Technology, Wuhan 430065, China*

*e. National-provincial Joint Engineering Research Center of High Temperature Materials and Lining Technology, Wuhan University of Science and Technology, Wuhan 430081, China*

**zuowei@wust.edu.cn*

**Abstract**: Accurate state-of-charge (SOC) estimation of lithium-ion battery is directly related to the reliability, performance, and safety of the battery. In this work, the second order resistor-capacitance (RC) circuit is equivalent to the battery model and the particle swarm optimization (PSO) algorithm is employed for achieving accurate identification of the parameters of circuit model under dynamic stress test (DST) conditions. Furthermore, the values of open circuit voltage (OCV) obtained from the identification results are input into the temporal convolutional network instead of the terminal voltages, and then the SOC of the Li-ion battery is estimated by directly learning the mapping relationship of OCV-SOC curves, which further improves the estimation accuracy and robustness of the proposed method. Finally, the SOC estimation is validated with the public dataset of $LiFePO_4$ batteries under all driving conditions at different temperature and compared with the individual TCN method. Results show that the SOC estimation of the second order resistor-capacitance circuit-PSO-TCN model is optimal with a root mean square error (RMSE) and maximum error (MAXE) less than 1.8% and 7.65%, respectively.

**Keywords:** Lithium-ion battery; State of charge estimation; Parameter identification; PSO algorithm; OCV-SOC curve; TCN

# Graphical Abstract (for review)

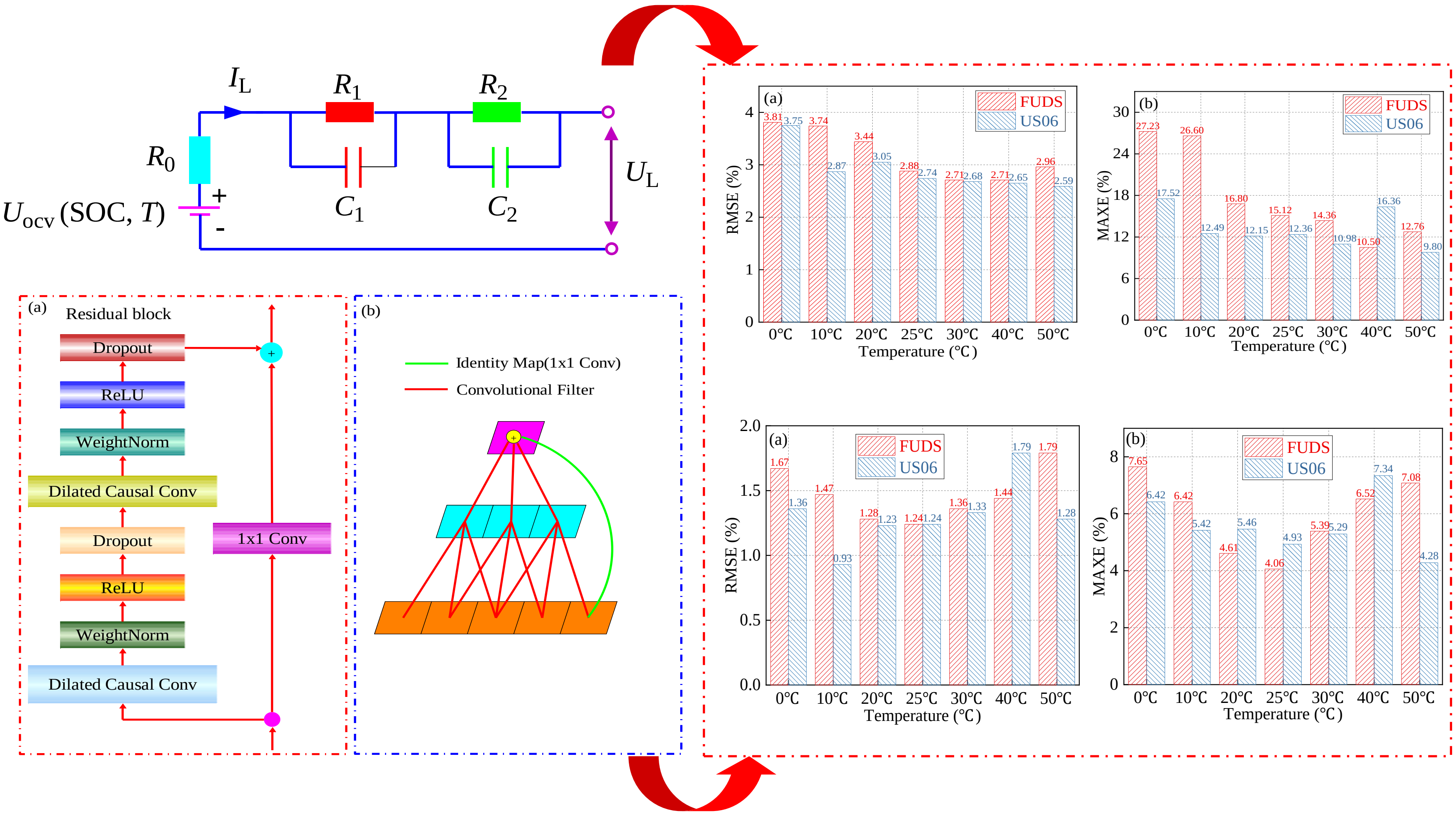

# Highlights

1. The second-order resistor-capacitance circuit is equivalent to the battery model.
2. Particle swarm optimization algorithm is employed for parameter identification.
3. SOC estimation is evaluated under all dynamic working conditions at different temperature.
4. RMSE and MAXE of the developed model are less than 1.8% and 7.65%, respectively.

**Nomenclature**

| | |
|---|---|
| AhI | Ampere hour integration |
| BMS | Battery management system |
| DAE | denoising autoencoder |
| ECM | Equivalent circuit model |
| EM | Electrochemical model |
| EKF | Extended Kalman filter |
| EVs | Electric vehicles |
| FUDS | Federal Urban Driving Schedule |
| GPR | Gaussian process regression |
| GRU | Gated recurrent unit |
| HIF | H-infinity filter |
| IFO | Improved fractional-order |
| IO | Integer-order |
| KF | Kalman filter |
| LIB | Lithium-ion battery |
| LSTM | Long short-term memory |
| MAXE | Maximum error |
| ML | Machine learning |
| NN | Neural network |
| OCV | Open-circuit voltage |
| PDEs | Partial differential equations |

| | |
|---|---|
| PF | Particle filter |
| PSO | Particle swarm optimization |
| RNN | Recurrent neural network |
| RF | Random forest |
| RMSE | Root mean square error |
| SOC | State of charge |
| SVM | Support vector machine |
| TCN | Temporal convolutional network |

# 1. Introduction

Due to the continuous warming of global climate [1-3] and incentives of domestic carbon-neutral policy [4-6], new energy vehicles have become a good choice for transportation tool instead of fuel vehicles [7, 8]. The wide applications of new energy vehicles are limited by Lithium-ion batteries [9], which are acted as the important power source for electric vehicles because of its good advantages such as high energy density, low self-discharge rate, long life, and zero emission [10, 11]. However, lithium-ion batteries under dynamic driving conditions are faced with many challenges [12], such as aging [13] and thermal runaway [14]. Therefore, advanced battery management systems (BMS) is necessary for monitoring and protecting the batteries.

The state of charge (SOC) of the battery is one of the most critical parameters in the battery management system (BMS) [15], which is defined as the ratio between the available capacity and the fully charged capacity of the battery [16]. Due to the nonlinearity, time-varying, and electrochemical reactions, obtaining the SOC value of a battery directly through sensor measurement is impossible [17]. It can be indirectly estimated by measurable signals such as temperature, voltage, current, and other measurable parameters [18]. In addition, the performance of batteries is highly affected by aging, temperature variations, and charging and discharging cycles [19], which makes accurately estimating the SOC very challengeable [20]. Therefore, it is particularly significant to develop advanced algorithms and strategies for accurate SOC estimation [21, 22].

## *1.1. Literature review*

At present, a considerable amount of research works have been done on SOC estimation at home and abroad. In general, methods for SOC estimation can be divided into four categories:

method based on mapping the representation parameters [23, 24], the ampere-hour integration method (AhI) [25], model-based estimation method [26-34], and data-driven method [35-46].

The characterization parameter-based method for SOC estimation is mainly divided into two steps. The first step is establishing the offline relationship between the power cell characterization parameters and SOC, and then calculating the values of power cell characterization parameter in real-time and calibrating the SOC value of power cell. Optional characterization parameters include impedance spectrum, and open-circuit voltage (OCV), etc. Usually, a relatively stable OCV-SOC relationship is used to calibrate the SOC of power batteries in industrial, which is simple and reliable. However, the biggest disadvantage of this method is that it requires the battery to be left standing for more than two hours until the terminal voltage is completely depolarized before SOC is estimated [23, 24].

The ampere-hour integration (AhI) method is a typical open-loop estimation method, which measures SOC by integrating the time-dependent discharge current. This method has the advantage of simplicity and ease of use, but it is highly depended on the initial value of SOC of the Li-ion battery. Meanwhile, when the accuracy of the current sensor is not high, the measurement error will accumulate over time, leading to a gradual deviation of the estimated value of SOC from the actual value [25]. In addition, the performance degradation of power battery leads to the degradation of static capacity, which affects the calculation accuracy of SOC.

The model-based approach consists of four steps: model selection, battery testing, identification of model parameters, and algorithmic estimation of SOC [26]. The most commonly used model for SOC estimation of Li-ion batteries is the equivalent circuit model (ECM) or electrochemical model (EM). The SOC estimation under electrochemical model is based on the porous electrode theory [27], which relies on a system of partial differential equations (PDEs) to describe the microscopic reactions inside the cell. EM can be accurate but will be accompanied by too much computation for real-time SOC estimation, and it will lead to high time complexity [28]. It is essential to reduce the number of parameters in the EM. Feng et al. [29] proposed an electrochemical-thermal neural network-based battery electro-thermal property model to further reduce the complexity of the neural network EM. The equivalent circuit model (ECM) involved fitting the battery characteristics through a circuit network composed of electronic components and combining it with a filtering algorithm to accomplish the SOC estimation of the power battery [30]. There are many types of filters available such as Kalman filter (KF), H-infinity filter (HIF), particle filter (PF), and sliding mode observer, among which the Kalman filter (KF) algorithm and its corresponding variant forms are the most widely used filtering algorithms in the model-based approach. He et al. [31] proposed an adaptive iterative extended Kalman filter method to estimate the SOC based on the Davignan circuit model, which takes into account effects of temperature on the battery capacity and the SOC-OCV relationship simultaneously and further improves the SOC estimation accuracy under the DST driving condition. Oluwole et al. [32] proposed an improved Fractional Order Extended Kalman Filter (IFO-EKF) based on integer order Extended Kalman Filter (IO-EKF) algorithm, which achieved more accurate SOC estimation under dynamic driving conditions, but its slow response time can only be applied offline. However, the SOC estimation is highly depended on the accuracy of the circuit model, where the model is usually not adaptable under different driving conditions [33, 34]. Besides, the errors from algorithmic in the above models are also not negligible, such as those caused by approximating a nonlinear system to a linear system using the extended Kalman filtering algorithm.

The SOC estimation based on data-driven methods doesn't require a comprehensive understanding of the internal characteristics of the battery and greatly avoids wasting time and effort to build complex battery models for showing the battery state [35-37]. Based on a large amount of offline data, this method establishes and trains a direct mapping relationship model between the current, voltage, temperature and SOC of power battery. Popular machine learning methods include support vector machine (SVM) [38], random forest (RF) [39], and Gaussian process regression (GPR) [40, 41]. However, the variation of SOC of lithium batteries is a continuous process since each SOC value is related to the previous information and the operation state is relatively complex. The above methods of SOC estimation performance are not as good as deep learning methods. Deep learning algorithms describe the nonlinear relationship between input and output by adjusting the number of layers and neurons. Popular deep learning methods include Long Short-Term Memory (LSTM), Gated Recurrent Unit (GRU), and Temporal Convolutional Networks (TCN) [42-44]. Chen et al. [45] introduced a denoising autoencoder neural network (DAE-NN) to extract useful data features by reducing the noise and increasing the dimensionality of the battery measurement data. Then, the feature-extracted data was used to train the GRU-RNN, which had been widely used for SOC estimation, and the model was verified to be highly accurate in SOC estimation under different working conditions. Hu et al. [46] proposed a temporal convolutional network (TCN) method to process the input data before the long short-term memory (LSTM) neural network. They demonstrated that the proposed TCN-LSTM method had better accuracy than the TCN and LSTM methods alone. Compared to LSTM and GRU, the TCN model had higher parallelism and fewer parameters when dealing with long sequence data, and could capture long-term dependencies more efficiently, and perform better in temporal sequence modeling tasks.

*1.2. Contributions of this work*

(1) A second order resistor-capacitance circuit-PSO-TCN model is proposed for SOC estimation. The model obtains the parameter identification results of the dynamic driving conditions at different temperatures through the particle swarm optimization algorithm, which is inputted into the TCN model through the corresponding transformations, and ultimately achieves the SOC estimation with high accuracy and robustness in $LiFePO_4$ batteries.

(2) Terminal voltage under the traditional data-driven model is replaced by OCV, making the TCN directly learn the OCV-SOC mapping relationship under the dataset of dynamic driving conditions, which enables the model to better adapt to the long-term dependencies in the sequential data, and provides an efficient and reliable solution for the SOC estimation application area.

(3) The proposed model is validated on the dataset of dynamic driving conditions at multiple temperatures and compared with traditional data-driven methods. The experimental results show that the method achieves satisfactory SOC estimation accuracy at all temperatures.

## 2. Methodology

*2.1. Battery circuit model*

The Li-ion battery is a relatively complex electrochemical system influenced by multiple factors such as physical and chemical processes. Meanwhile, it is highly nonlinear, making it challengeable to accurately model the interior of lithium batteries [47]. Equivalent circuit model is widely used in electric vehicles and modeling and simulation of drive systems since they are better adapted to the various operating states of the battery and the state equations of the model can be derived for easy analysis and application [48]. Common equivalent circuit models include the Rint model [49], the PNGV model [50], the Thevenin model [51], and the n-RC equivalent circuit model

[52]. The Rint model is an ideal model that ignores the resistive and capacitive properties of the battery, making it difficult to accurately describe the polarization inside the battery. In contrast, the PNGV model has a clear physical interpretation and is easy to be calculated. However, the conventional PNGV model has fixed cell parameters, which are actually related to the SOC of the cell, making it difficult to ensure accurate estimation of SOC in practical applications. Although the Thevenin model introduces the RC network, it still cannot fully describe the polarization phenomenon of the battery [53]. With the above comparison, the second-order RC equivalent circuit model is more effective in describing the polarization phenomenon of the battery and is relatively easy for parameter identification, which has been widely used in practical applications [54]. Thus in this work, the second-RC equivalent circuit model is used to describe the dynamic behavior of the battery.

Figure 1 illustrates the structure of the model, which consists of three main parts: (a) Voltage source: $U_{\mathrm{OCV}}$ represents the open-circuit voltage of the cell, which is considered as a function of SOC and the current temperature $T$. It indicates the OCV of the cell under different driving conditions, i.e. OCV=$f$ (SOC, $T$). To achieve a high accuracy, the polynomial function in Equation (1) is adopted and it is parameterized to quantitatively describe the nonlinear OCV-SOC relationship [55]:

$$\mathrm{OCV_{SOC}} = P_1 * \mathrm{SOC}^7 + P_2 * \mathrm{SOC}^6 + ...... + P_6 * \mathrm{SOC}^2 + P_7 * \mathrm{SOC} + P_8 \qquad (1)$$

(b) Ohmic resistance: $R_0$ denotes the internal resistance of the electrodes, electrolyte, and spacer as well as the contact resistance of the components. (c) Second-order RC network: $Ri$ denotes the polarization resistance and $C_i$ denotes the polarization capacitance, which is used to describe the polarization effect during the charging and discharging phases.

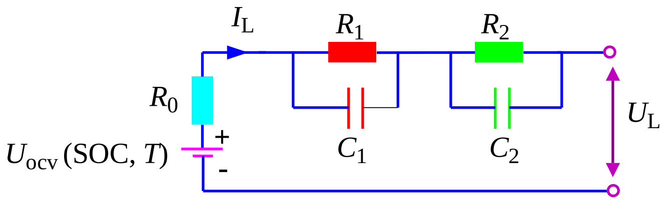


Figure 1 Second order RC model

The dynamic electrical behavior can be described by Equations (2) and (3), whose discrete-time state-space equations can be rewritten as Equations (4) and (5).

$$\bar{U} = \frac{i_0}{C_p} - \frac{U_p}{\tau} \tag{2}$$

$$U_t = U_{oc} - U_p - i_0 R_0 \tag{3}$$

$$U_{p,k+1} = \exp(-\frac{\Delta t}{\tau_k}) U_{p,k} + (1 - \exp(-\frac{\Delta t}{\tau_k})) R_p i_{0,k} \tag{4}$$

$$U_{t,k} = U_{oc,k} - U_{p,k} - i_{0,k} R_{0,k} \tag{5}$$

where $\tau$ denotes the time constant of the RC branch, $\tau = R_p \times C_p$. It is worthy noted that the subscript $k$ denotes the moment $k$. $\Delta t$ is the sampling time, which is equal to 1s in this study, and $U_t$ and $U_p$ denote the terminal voltage and the polarization voltage of the capacitor $C_p$, respectively. In addition, $i$ denotes the load current [56].

## *2.2. Particle swarm optimization algorithm*

Particle swarm optimization (PSO) algorithm belongs to a typical bio-inspired swarm intelligence optimization algorithm that iteratively searches for the global optimal solution in a complex search space through cooperation and competition among particles [57]. At each iteration, particles update their velocity and position based on individual and global optimal values [58]. Now assume that there exists an N-dimensional search space with a total of m particles forming a particle swarm $X$=[$X_1$, $X_2$, …, $X_m$]$^T$ and the position of a particle represents a potential optimal solution to the problem, the velocity of the ith particle is: $Vi$=[$V_{i1}$, $V_{i2}$, …, $V_{iN}$]$^T$, the individual extremum of the particle is: $P_i$=[$P_{i1}$, $P_{i2}$, …, $P_{iN}$]$^T$, and the population extremum of the particle swarm is: $Pg$=[$P_{g1}$, $P_{g2}$, …, $P_{gN}$]$^T$. The velocity and position formulas are shown below:

$$V_{\mathrm{in}}^{k+1} = wv_{\mathrm{in}}^{k} + c_1 r_1 (P_{\mathrm{in}}^{k} - X_{\mathrm{in}}^{k}) + c_2 r_2 (P_{\mathrm{gn}}^{k} - X_{\mathrm{in}}^{k}) \tag{6}$$

$$X_{\mathrm{in}}^{k+1} = X_{\mathrm{in}}^{k} + V_{\mathrm{in}}^{k+1} \tag{7}$$

where $n$=1, 2, ..., $N$, $i$=1, 2, ..., $m$, $k$ is the number of iterations at this time, and $V_{\mathrm{in}}$ is the speed of the particle. $w$ is the inertia weight. The larger the weight, the stronger the global search capability of algorithm, the faster the search speed. The smaller the weight, the stronger the local optimization capability of the algorithm. $c_1$, $c_2$ is the acceleration factor, which is the non-negative constant. $c_1$ represents the maximum step length of the particle to the individual optimal position. $c_2$ is the maximum step length of the particle to the global optimal position. If the acceleration factor is larger, the particle can quickly approach the optimal position. Else if it is too small, it is easy to cause the particles to stagnate at a certain position, and cannot search for the optimal position. $r_1$ and $r_2$ are the random numbers between 0 and 1, which influence the diversity of the particle swarm, and ensures that the algorithm will not lose the diversity in the iterative calculation.

### *2.3. TCN model*

The TCN model belongs to the convolutional network and realizes memory history feature extraction applicable to sequential data by using improved techniques such as causal convolution, dilated convolution, and residual block [59]. Its special network structure not only has the advantages of flexible perceptual field size, low memory consumption, and parallel computation but also avoids the problem of gradient vanishing or gradient explosion in RNN training [60].

#### *2.3.1. Dilated convolution*

Since the length of time series modeled by the conventional convolutional neural network is limited by the size of the convolutional kernel as well as the depth of the network structure, a linear stacking of more layers is required if the longer and more complex temporal dependency is handled. In the *n*-layer structure of a standard convolutional network, the size of the convolutional kernel is *k*, and the size of the computed receptive field *RF* is expressed as follows:

$$RF = n*(k-1)+1 \tag{8}$$

By introducing the extended convolutional structure, the relationship between the sensory field range of the neural network and the number of hidden layers changes from linear to exponential. As a result, the model can obtain a larger sensory field range while maintaining a shallower network depth, which makes it easier to optimize and converge [61]. Meanwhile, the formula for the feeling field range *y* becomes as follows:

$$y = \sum_{n=1}^{n}(k-1)*d_n + 1 \tag{9}$$

where *n* represents the number of hidden layers, *k* represents the size of the convolutional kernel, and $d_n$ represents the unfolding factor of the *n*th hidden layer, which is computed as $d_n=2^{n-1}$. Figure 2 illustrates an inflated convolutional network with 3 layers, and the range of receptive field increases significantly with the number of network layers.

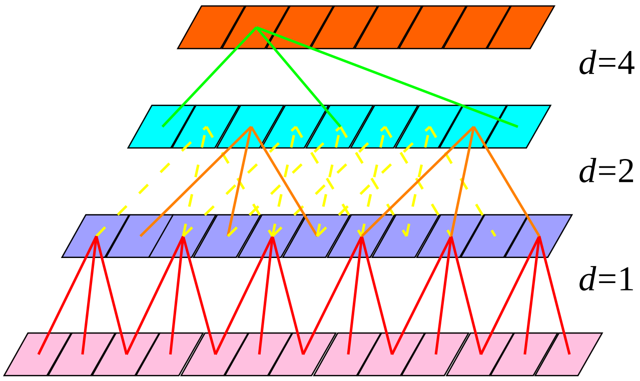


Figure 2 Dilated convolution

### *2.3.2. Causal convolution*

Causal convolution means that the output of each time step depends on previous time steps, and for the value of the previous layer at moment $t$, it only depends on the value of the next layer at moment $t$ and before. Figure 3 illustrates the causal convolutional model containing 2 hidden layers and a convolutional kernel size of 2. Be different from the traditional convolutional neural network, the causal convolution cannot see future data. It is a unidirectional structure, not bidirectional, and it is a strictly time-constrained model. In other words, in the case where the time series is $X=(x_1, x_2, \ldots, x_T)$ and the filter $F=(f_1, f_2, \ldots, f_K)$, the causal convolution at $x_t$ can be expressed as:

$$f(x_t) = \sum_{k=1}^{K} f_k x_{t-K+k} \tag{10}$$

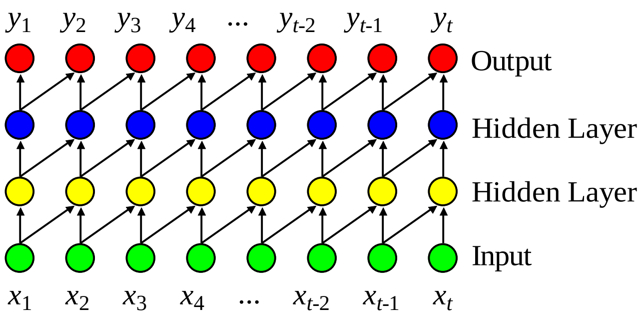


Figure 3 Causal convolution

### *2.3.3. Residual block*

Residual connection is a technique for transferring information by adding cross-layer connections to a network model, where input signals can be passed directly to the outputs of subsequent layers through connections across the layers. This mechanism of residual connections allows the network to better capture the differences between inputs and outputs, which helps to speed up the network training process and avoid problems such as gradient explosion or gradient vanishing even if the network is too deep [62]. By introducing residual connectivity, TCN can better convey and utilize historical information, improving the ability to model time series data.

Figure 4 illustrates the residual block in the TCN. Figure 4(a) shows the various components of the residual block, where the left branch consists of two one-dimensional causal convolutional and weight normalization layers and the Dropout layer, activated by the ReLU function. The right branch represents the residual connection. To ensure that the outputs of both branches have the same dimensionality, a one-dimensional convolution operation is used to control the data dimensionality. Figure 4(b) summarizes the full picture of residual connectivity in TCN neural network. As described in the literature [63], the output equation of the residual block can be expressed as follows:

$$y = h(f(x) + Conv1D(x)) \tag{11}$$

where $y$ is the output of the residual block, $x$ is the input of the residual block, $f(\bullet)$is a series of transformation operations represented by the left branch, $Conv1D(\bullet)$ is a one-dimensional convolution operation, and $h(\bullet)$ represents the activation function ReLU.

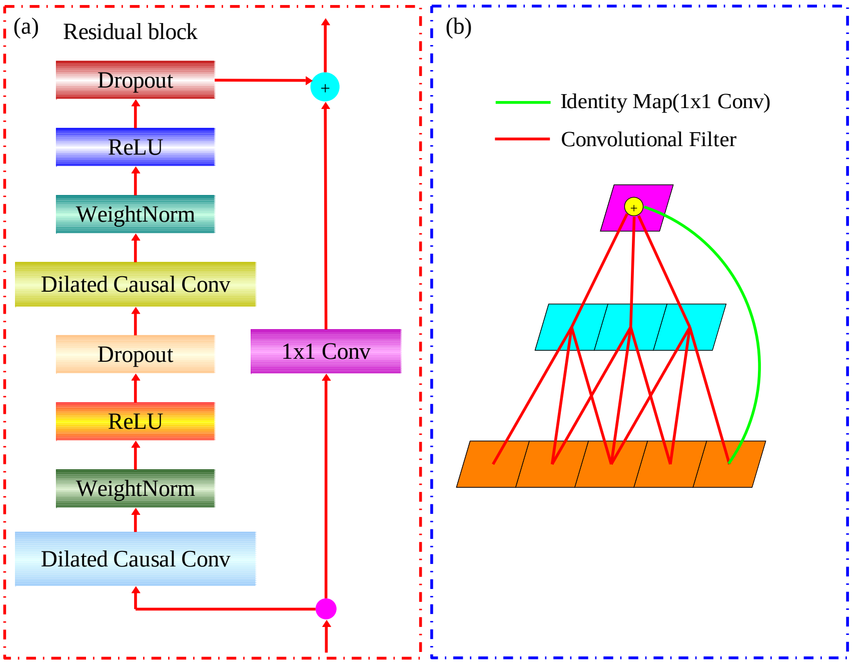


Figure 4 Residual block

## 3. Data processing and evaluation criteria

### *3.1. Dataset of sample*

The actual driving conditions of electric vehicles are complex and uncertain. To be closer to the real situation when simulating the battery load condition of EVs, different test data sources are used to enrich the training dataset. Specifically, the training data from dynamic stress test (DST) profiles is applied, which is the simplification of actual driving conditions but account for regenerative charging. Then, in order to assess the generalization ability of the SOC estimation method, i.e. the estimation performance on unknown data, data sources that are very different from the training data are chosen as test data. These data sources including the US06 Driving Regulations are used to simulate highway driving conditions, and the Federal Urban Driving Regulations (FUDS) are used to simulate urban roadway driving conditions. With this approach, the performance of the SOC estimation method can be assessed more comprehensively to ensure that it performs well under various driving conditions. This comprehensive approach helps to improve the reliability and efficiency of EV battery management systems. For more detailed information, the U.S. Advanced Battery Consortium (USABC) manual can be referenced [64].

In this work, the public dataset of the A123 battery cell from the University of Maryland Center for Advanced Life Cycle Engineering (CALCE) database [65] is selected, and the specific information of this battery cell is shown in Table 1. The dataset records the variation of voltage, current, and temperature of EV batteries at temperatures from -10°C to 50°C. Although the $LiFePO_4$ battery dataset provides data on operation at negative temperatures, it should be noted that the dynamic characteristics of the battery are very unstable at negative temperatures. This instability will greatly increase the difficulty of SOC estimation and might have an impact on the lifespan of the battery, so the battery data at 0 -50 °C is selected as the data set for this simulation. The dataset contains three observations under three EV driving conditions, including DST, US06, and FUDS. Figures 5, 6, and 7 depict the current, voltage, temperature, and SOC distribution curves for the three driving conditions at 30 °C.

Table 2 Parameters of A123 battery cells

| Type | A123 Battery |
|---|---|
| Cell Chemistry | $LiFePO_4$ |
| Nominal Capacity | 1.1Ah |
| Nominal Voltage | 3.2V |
| Weight | 76g |
| Diameter | 25.4mm |
| Length | 65mm |
| Charge cut-off voltage | 3.6V |
| Discharge cut-off voltage | 2.0V |

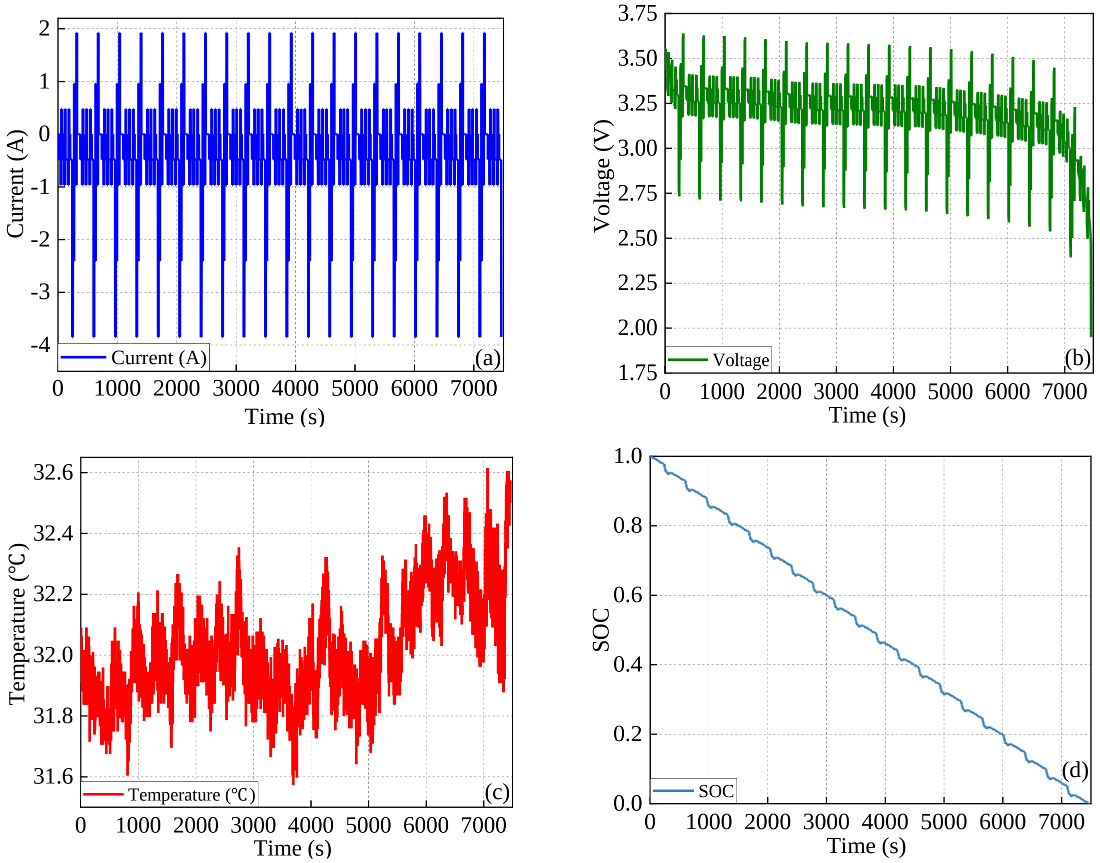


Figure 5 Driving condition of DST at 30 ℃: (a) current; (b) voltage; (c) temperature; (d) SOC.

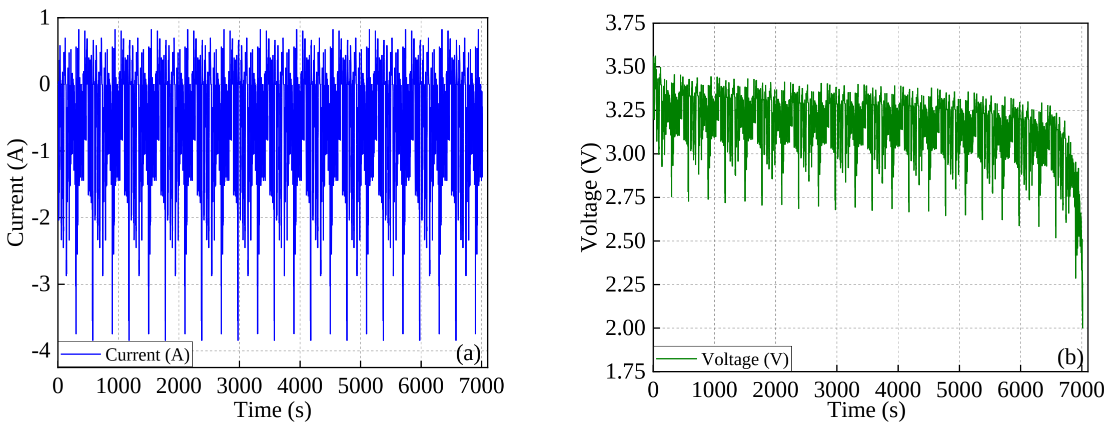

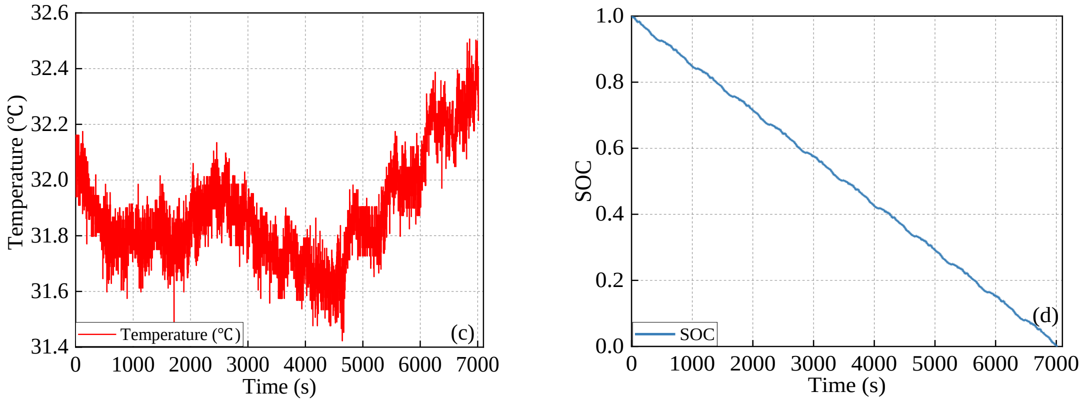


Figure 6 Driving condition of US06 at 30 ℃: (a) current; (b) voltage; (c) temperature; (d) SOC

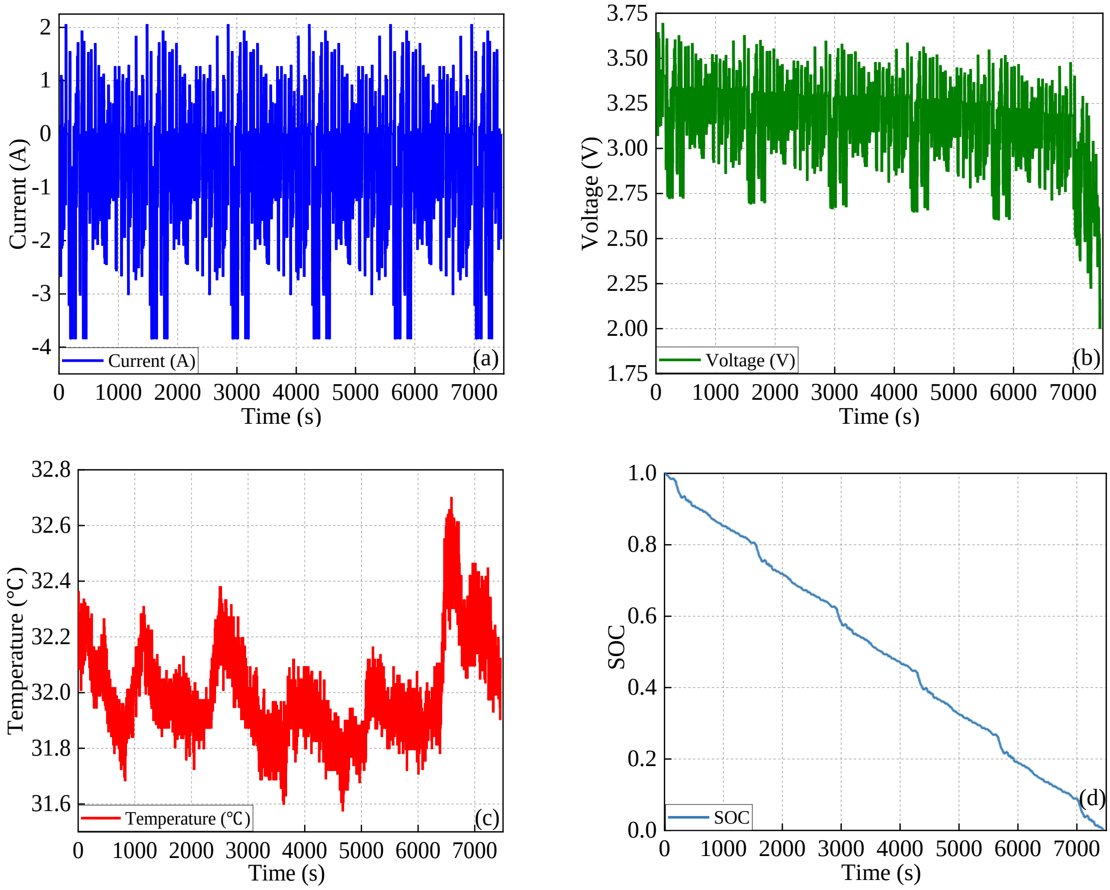


Figure 7 Driving condition of FUDS at 30 ℃: (a) current; (b) voltage; (c) temperature; (d) SOC

### *3.2. Data preprocessing*

To improve the training efficiency and robustness of the network, it is necessary to normalize the battery measurement data (voltage, current, temperature). Therefore, the min-max normalization method is used to map the battery measurement data of the above four datasets to the interval [-1, 1]. The related equation is expressed as follows:

$$x_{\text{norm}} = \frac{2(x_{\text{orig}} - x_{\text{min}})}{x_{\text{max}} - x_{\text{min}}} - 1 \tag{12}$$

where $x_{\text{max}}$ and $x_{\text{min}}$ are the maximum and minimum values of the measured variables in the dataset, respectively, $x_{\text{orig}}$ is the original value, and $x_{\text{norm}}$ is the corresponding normalized value, namely the actual input data of the network.

### 3.3. Evaluation criteria

Two parameters are used to evaluate the SOC estimation performance of the method, i.e., Root Mean Square Error (RMSE) and Maximum Error (MAXE), which are defined as follows:

$$\text{RMSE} = \sqrt{\frac{1}{N}\sum_{i=1}^{N}(\text{soc}_{\text{real}} - \text{soc}_i)^2} \tag{13}$$

$$\text{MAXE} = \max(|\,\text{soc}_{\text{real}} - \text{soc}_i\,|), 1 \le i \le N \tag{14}$$

where $N$ is the total number of samples, $\text{soc}_{\text{real}}$ is the true value of SOC derived from the Coulomb counting method, and $\text{soc}_i$ is the estimated value from the SOC estimation method. RMSE denotes the robustness of the estimation results, while MAXE denotes the extreme results.

## 4. Results and discussions

### 4.1. $LiFePO_4$ battery parameter identification

Because of the strong nonlinear relationship between OCV and SOC of Li-ion batteries, the vast majority of SOC estimation methods essentially estimate the SOC of Li-ion batteries through the mapping relationship of OCV-SOC curves. The estimation accuracy of Li-ion battery model parameters directly affects the OCV of the battery, and there is a long flat interval in the normal discharge stage of the $LiFePO_4$ battery used in this work, i.e., it indicates that a very small voltage estimation error may lead to a large SOC estimation error [66]. Therefore, this subsection adds the

PSO algorithm to achieve accurate identification of the second-order RC circuit model under dynamic driving conditions. Firstly, OCV-SOC relationship is polynomially fitted based on the low-current discharge data, and then the battery data with SOC of 20-80% under the driving condition of DST is selected as the experimental data, the parameters to be identified include ψ=[R0, R1, C1, R2, C2], in which the size range of the ohmic internal resistance, R0, is [0.01Ω-1Ω], and the size range of the polarization internal resistances, R1, R2 size range is [0.001Ω-0.1Ω], polarization capacitance C1, C2 size range is [500F-5000F]. The process of the PSO algorithm optimizing the second-order RC circuit model is illustrated in Figure 8, and the final results of the optimal parameters are shown in Table 3, while Figure 9 and Figure 10 shows the OCV curves at 0 °C and 25 °C under different driving conditions according to the parameter identification results. The specific steps are indicated as follows:

1. Define the parameter space: firstly, determine the parameters ψ=[R0, R1, C1, R2, C2] of the optimized second-order circuit model. These hyperparameters include the ohmic internal resistance R0, the polarization internal resistance R1, R2, and the polarization capacitance C1, C2. Determine the range of values for each parameter as the appropriate search space.

2. Initialize the particle swarm: determine the initial position and velocity of the particles, each particle represents a set of parameters of the circuit model, and the initial parameters can be generated randomly. In this work, the selected particle swarm dimension is 5, and the number of particle swarms is 75.

3. Define the fitness function: construct and discretize the circuit equations (Equations (2)-(5)) using parameter settings, evaluate the performance of the network by appropriate evaluation metrics, and calculate the individual and global extremes based on the fitness values of the particles. In this work, the mean square error is used to represent the optimal fitness function of the particle swarm

optimization algorithm with the following equations:

$$fit = \frac{1}{T}\sum_{t=1}^{T}(\text{Voltage}'(t) - \text{Voltage}(t))^2 \tag{15}$$

where $T$ is the size of the selected sample, $t$ is the number of sequences of particles, Voltage'($t$) is the predicted output of the terminal voltage, and Voltage($t$) is the true output of the terminal voltage.

4. Update the velocity and position of particles: update the velocity and position of each particle according to Equation (6) and Equation (7), and then calculate the adaptation value based on the new position to update the individual extreme value and global extreme value.

5. Update the particle's best position and global best position: for each particle, compare its current fitness value with its individual best fitness value. If the current fitness is better, update the individual best position to the current position. Meanwhile, compare the individual best fitness values of all particles and take the position of the particle with the best fitness as the global best position.

6. Determine whether the iteration termination conditions are met, if the results meet the requirements, the algorithm ends and outputs the optimal results of the parameters of the second-order RC circuit model, otherwise, return to step 3.

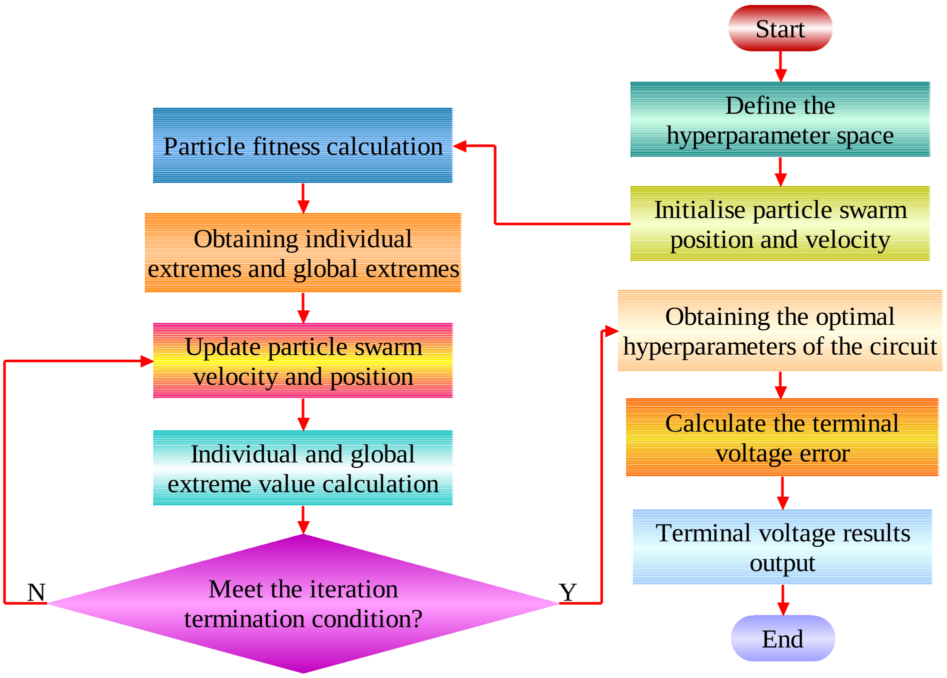


Figure 8 PSO algorithm for parameter identification

Table 3 Parameter identification results at different temperatures

| Temperature (℃) | R0 (Ω) | R1 (Ω) | C1 (F) | R2 (Ω) | C2 (F) |
|---|---|---|---|---|---|
| 0℃ | 0.19522 | 0.059145 | 4651.315 | 0.038954 | 608.212 |
| 10℃ | 0.17274 | 0.033854 | 1223.49 | 0.017505 | 7758.53 |
| 20℃ | 0.15729 | 0.01397 | 3177.315 | 0.017411 | 1139.27 |
| 25℃ | 0.15652 | 0.020377 | 997.975 | 0.001056 | 4585.86 |
| 30℃ | 0.15136 | 0.01589 | 848.695 | 0.00116 | 7165.34 |
| 40℃ | 0.14932 | 0.00936 | 874.274 | 0.001038 | 2189.58 |
| 50℃ | 0.14852 | 0.01256 | 1773.57 | 0.00836 | 2153.48 |

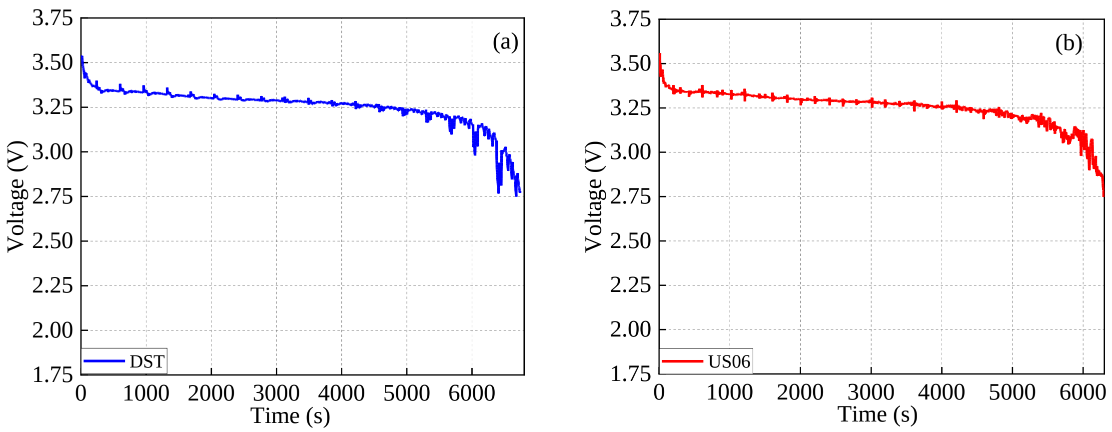

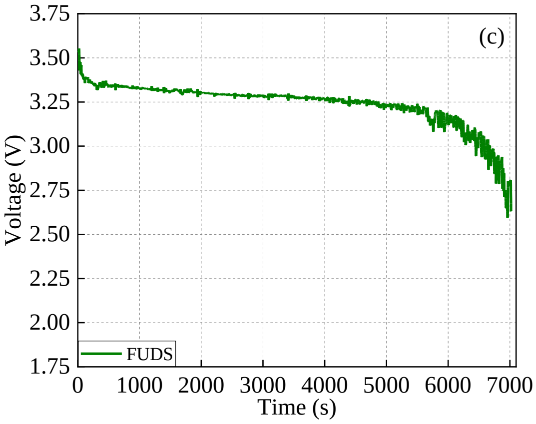


Figure 9 OCV estimation curves for different driving conditions at 0°C: (a) DST; (b) US06; (c) FUDS

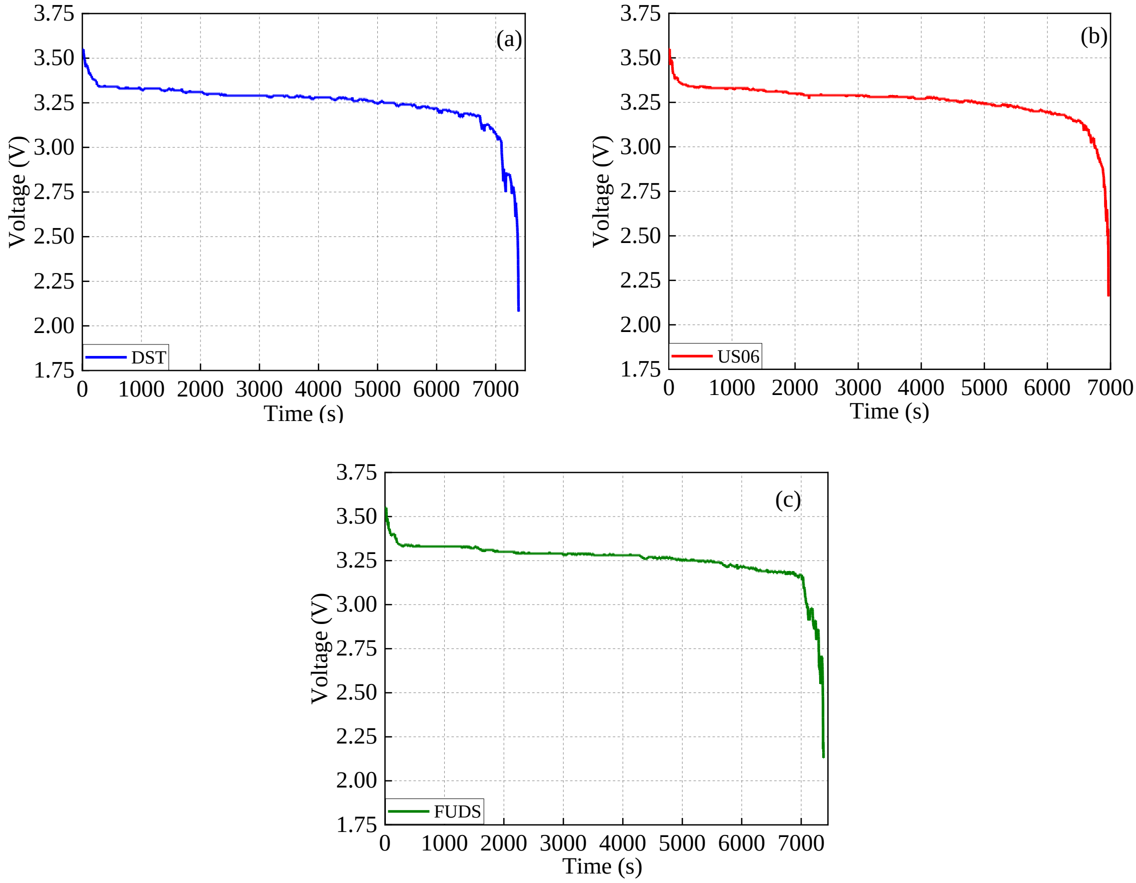


Figure 10 OCV estimation curves for different driving conditions at 25°C: (a) DST; (b) US06; (c) FUDS

*4.2. SOC estimation under TCN model*

This subsection mainly validates the performance of the individual TCN model in SOC estimation. Firstly, the TCN model using DST datasets at different temperatures (0°C, 10°C, 20°C, 25°C, 30°C, 40°C, 50°C) to test the US06, FUDS driving conditions at the same temperatures are used as the validation set and test set respectively to validate the generalization ability of the model, the network hyperparameters are set as shown in Table 4.

Table 4 Hyperparameters of TCN model for SOC estimation

| Parameters | Value |
|---|---|
| Learning rate | 0.0025 |
| Kernel_size | 9 |
| Number of convolution kernels | 62 |
| Number of residual blocks | 3 |
| Training epoch | 1000 |
| Optimizer | Adam |

Figures 11 and 12 suggest the SOC estimation results of the TCN model for the FUDS and US06 driving conditions at 10°C, 20°C, 40°C, and 50°C. The results show that the TCN model has the ability to capture the SOC trends of unknown working conditions at different temperatures relatively well, which validates the generalization ability of the TCN model. Figure 13 demonstrates the error results of the TCN model under US06 and FUDS conditions at temperatures from 0 to 50 °C, where the true SOC values are derived from the ampere-hour integration method. It can be seen that the RMSE of the TCN model for SOC estimation is all within 4%. However, the maximum error is greater than 20%, which implies that the SOC estimation results are less robust. Overall, there are two components that contribute to the large errors. The first is that when the battery at a lower temperature, the battery will experience greater fluctuations of voltage, leading to unstable characteristics within the battery and making it difficult to establish an accurate correlation between SOC and voltage. The second is that when the $LiFePO_4$ battery is located in the flat period (within the SOC between 30% and 70%), there is a significant fluctuation between the predicted and true values of SOC, which is attributed to the weak nonlinear mapping capability between the measured variables of the battery and the SOC in this period.

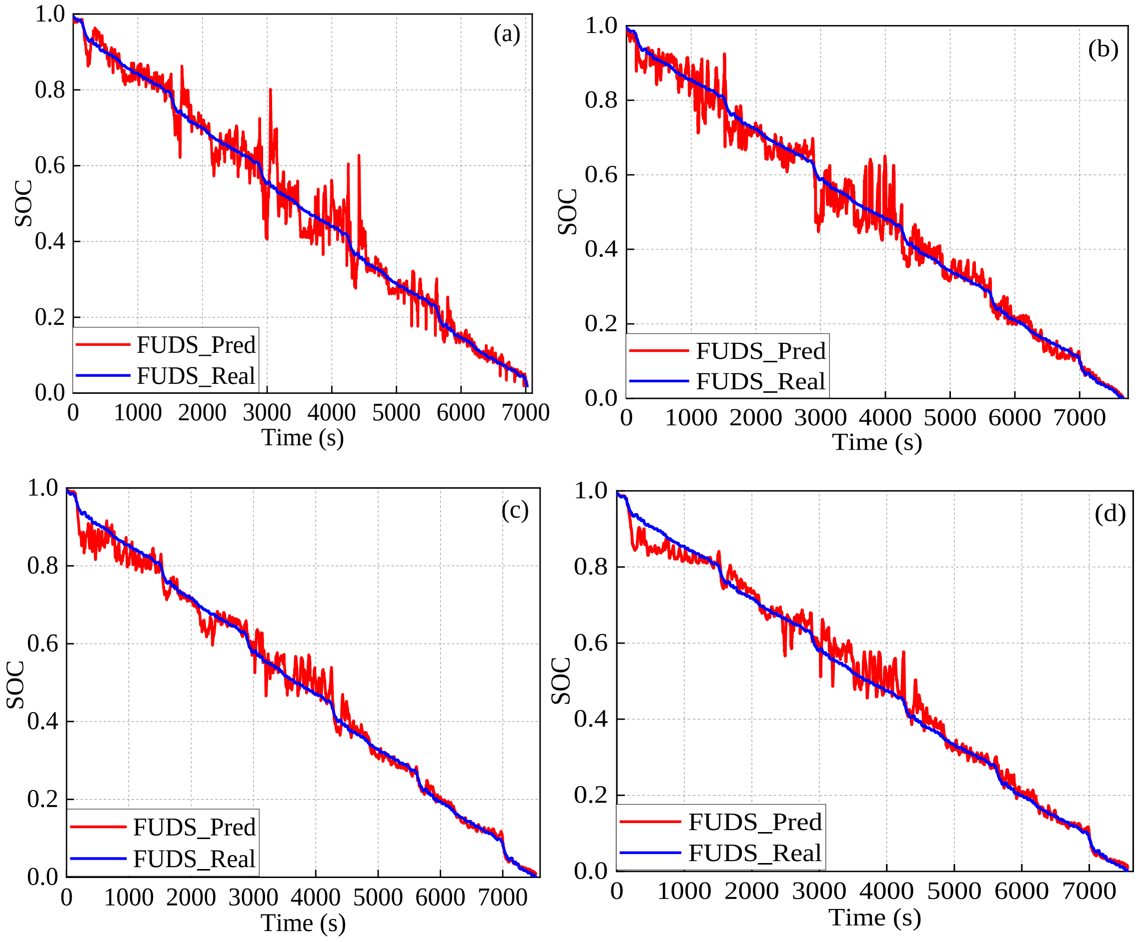


Figure 11 SOC estimation by TCN model for FUDS at different temperature: (a) 10 °C; (b) 20 °C; (c) 40 °C; (d) 50 °C

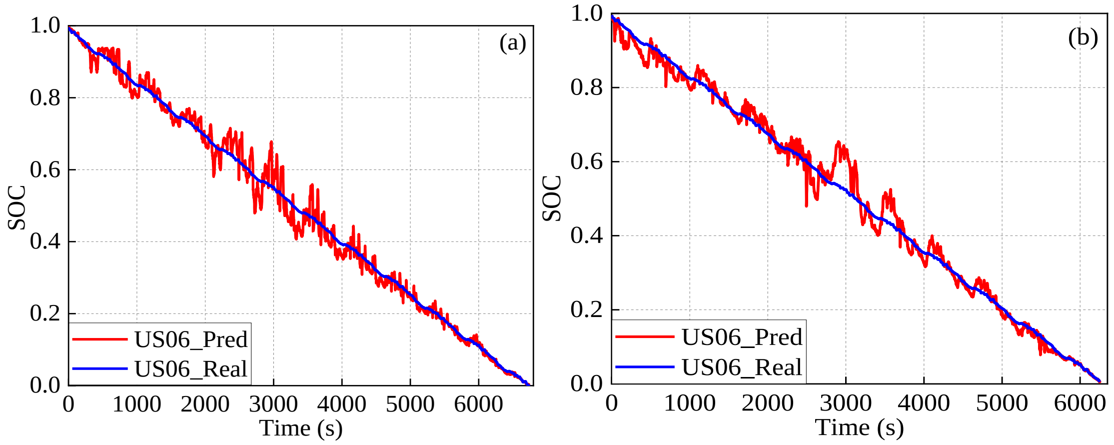

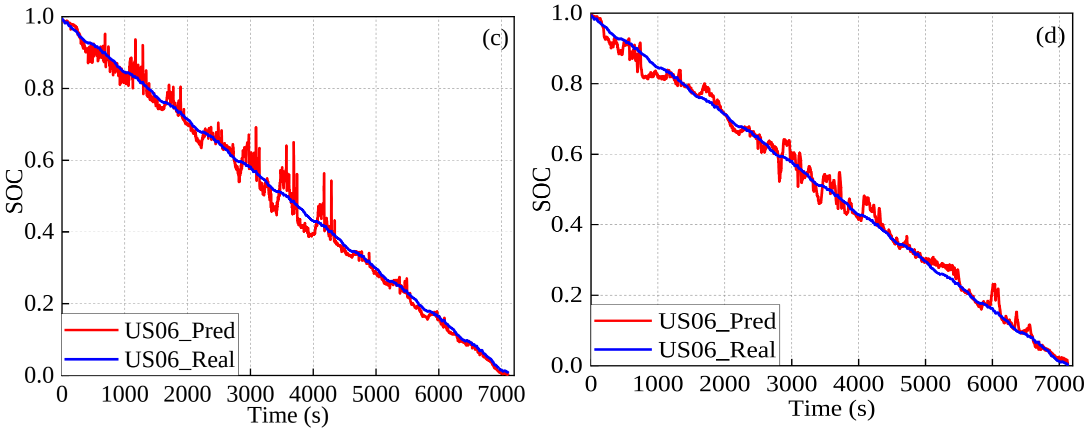


Figure 12 SOC estimation by TCN model for US06 at different temperature: (a) 10 °C; (b) 20 °C; (c) 40 °C; (d) 50 °C

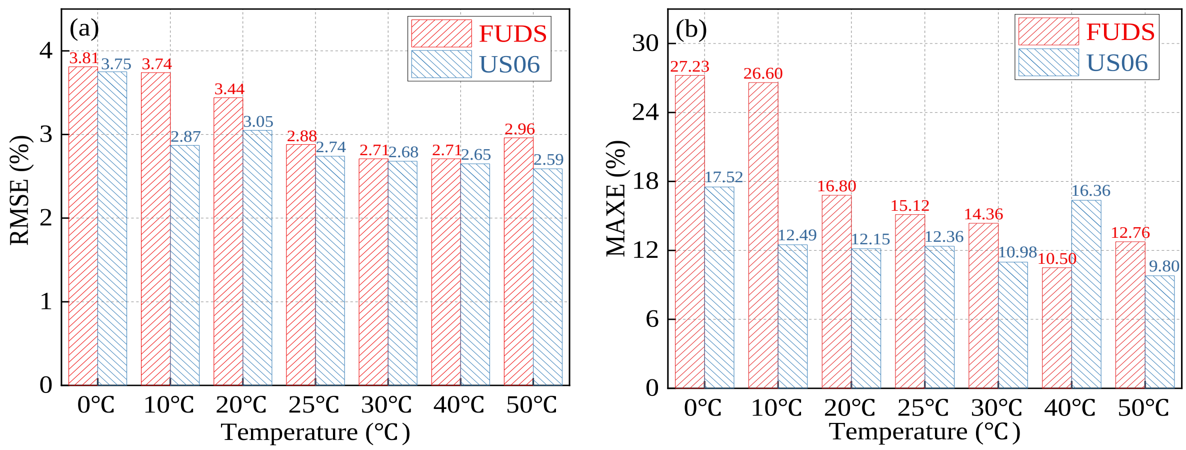


Figure 13 SOC estimation error by TCN model for US06 and FUDS at different temperature: (a) RMSE; (b) MAXE

*4.3 SOC estimation under second order resistor-capacitance circuit-PSO-TCN model*

In the previous subsection, the SOC estimation of the Battery data at different temperature and driving conditions is performed by the individual TCN model and the results show that the individual TCN model exhibits excellent generalization ability in this data. However, the RMSE of the output SOC of the individual TCN model is still as high as 4%, and in particular, the MAXE is still as high as 27%. Therefore, the SOC estimation accuracy and stability need to be further improved to meet the demands of practical applications. In this subsection, the OCV value of the battery at each moment in time is estimated by using the results after parameter identification at different temperature, and the OCV obtained after estimation is used as one of the inputs to the TCN model for replacing the conventional terminal voltage value.

Figures 14 and 15 show the SOC estimation results by using the OCV resulting from the parameter identification as inputs to the TCN, and the validation is performed under the US06 and FUDS conditions, respectively. By comparing Figures 11 and 12 with Figures 14 and 15, it can be seen that SOC estimation by the improved method not only learns the trend of SOC variation at all temperatures very well but also smoothes the output of SOC estimation by the individual TCN model. The results of the SOC estimation errors performed by the improved method at all temperatures are shown in Figure 16, which indicates that the improved method can further reduce the SOC estimation errors at different temperature compared to the individual TCN model. In particular, the RMSE is reduced from 3.8% to 1.8% and the MAXE is reduced from 27% to 7.4%. In summary, the improved method is an effective way to improve the accuracy and stability of SOC estimation.

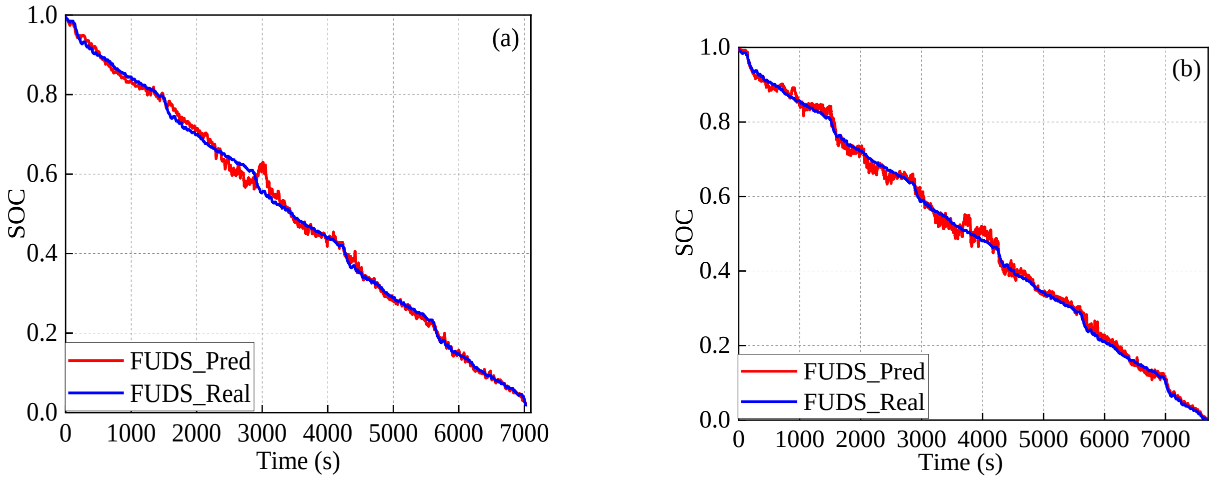

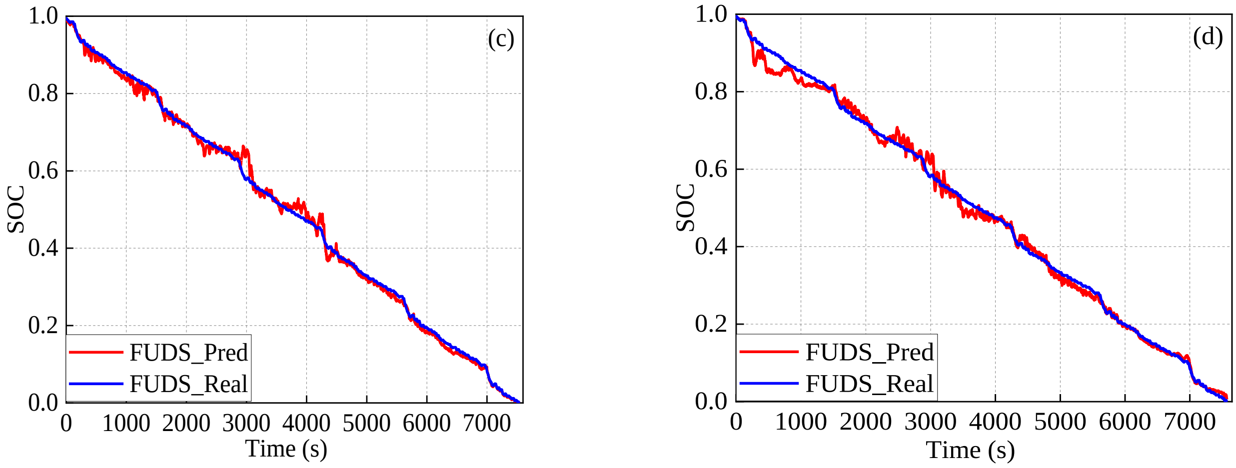


Figure 14 SOC estimation by the second order resistor-capacitance circuit-PSO-TCN model for FUDS at different temperature: (a) 10 °C; (b) 20 °C; (c) 40 °C; (d) 50 °C

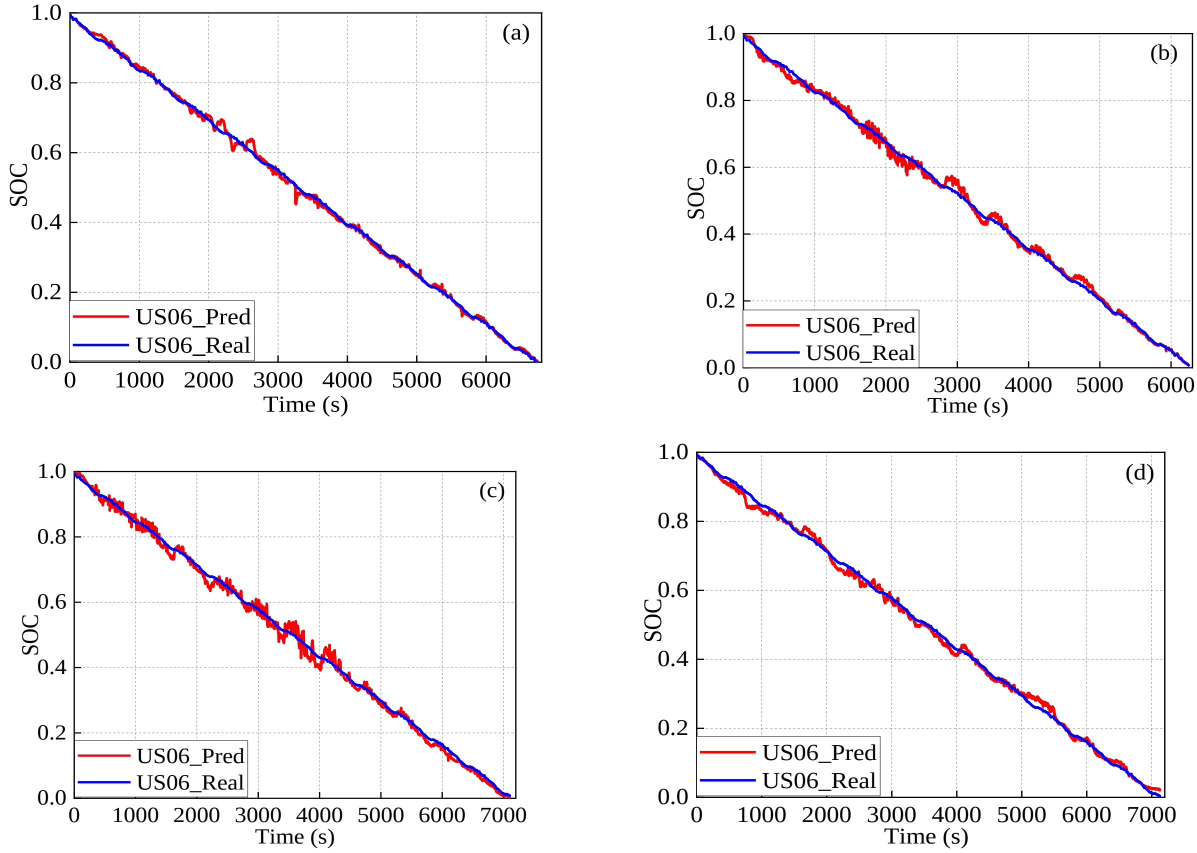


Figure 15 SOC estimation by the second order resistor-capacitance circuit-PSO-TCN model for US06 at different temperature: (a) 10 °C; (b) 20 °C; (c) 40 °C; (d) 50 °C

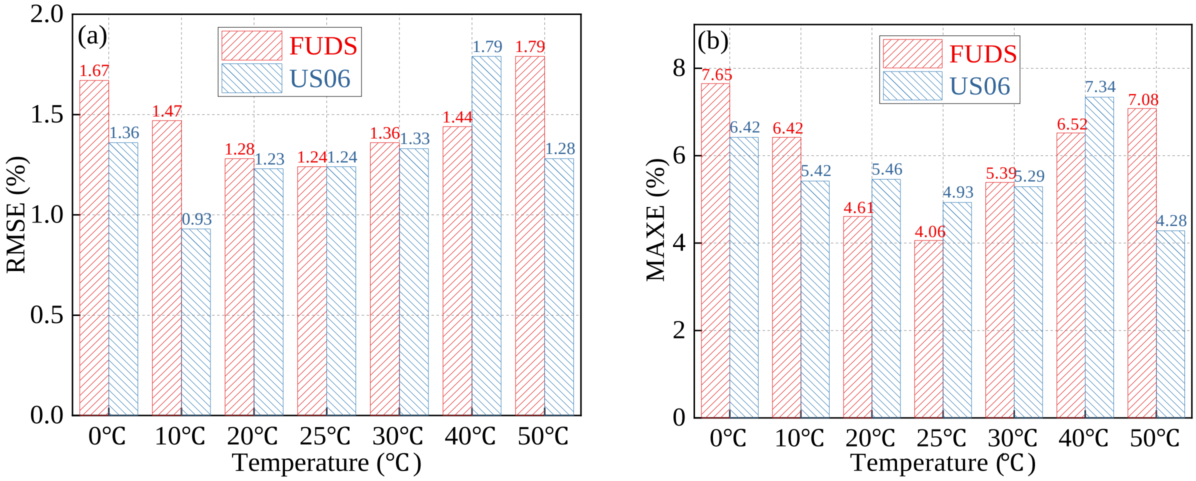


Figure 16 SOC estimation error by the second order resistor-capacitance circuit-PSO-TCN model for US06 and FUDS at different temperature: (a)RMSE; (b)MAXE

## 5. Conclusions

In this work, based on the characteristics of Li-ion batteries, a second-order RC circuit model is constructed and the PSO algorithm is used to accurately identify the model parameters. The OCV value of batteries at each moment is ultimately obtained by the discretized circuit equations. The TCN model is used to directly learn the OCV-SOC mapping relationship, and the performance and generalization ability of the developed SOC estimation method under different temperatures and driving conditions are validated by the public dataset of $LiFePO_4$ battery. The superior performance of the developed method is validated by comparing the SOC estimation results of the individual TCN model under the same battery dataset. The results show that changing the input variable for SOC estimation by the traditional data-driven approach, i.e., transforming the terminal voltage into the OCV value of the Li-ion battery, is able to help the network better learn the mapping relationship related to the internal characteristics of the battery and reduce the fluctuation of the output SOC. Compared with the results of SOC estimation by the individual TCN model, the proposed model shows a substantial improvement in SOC estimation capability at different temperature, leading to accurate SOC estimation of Li-ion battery. Specifically, the developed model shows excellent performance in the unknown driving conditions such as FUDS and US06, where RMSE and MAXE are less than 1.8% and 7.65%, respectively. As a result, the second order resistor-capacitance circuit-PSO-TCN model in this work is highly practical.

## Conflict of Interests

None declared.


## Acknowledgments

Dr. Wei Zuo gratefully acknowledges the financial support provided by Natural Science Foundation of Hubei Province (No. 2023AFB029), China Scholarship Council (No. 202308420174), National Natural Science Foundation of China-Hubei Joint Fund (No. U22A20127) and Wuhan Yellow Crane Talents Program. Dr. Yuhan Huang is a recipient of the ARC Discovery Early Career Research Award (DE220100552).


## References


[1] Sun Y, Cai T, Zhao D. Thermal performance and NO*x* emission characteristics studies on a premixed methane-ammonia-fueled micro-planar combustor Fuel 2021;291:120190.

[2] Zhao D. A real-time plane-wave decomposition algorithm for characterizing perforated liners damping at multiple mode frequencies. The Journal of the Acoustical Society of America 2011;129(3):1184-1192.

[3] Sun Y, Zhao D, Ji C, Zhu T, Rao Z, Wang B. Large-eddy simulations of self-excited thermoacoustic instability in a premixed swirling combustor with an outlet nozzle. Physics of Fluids 2022 34(4):044112.

[4] Cai T, Zhao D, Chan S H, Shahsavari M. Tailoring reduced mechanisms for predicting flame propagation and ignition characteristics in ammonia and ammonia/hydrogen mixtures. Energy

2022;260:125090.

[5] Ni S, Zhao D. NO*x* emission reduction in ammonia-powered micro-combustors by partially inserting porous medium under fuel-rich condition. Chemical Engineering Journal 2022;434:134680.

[6] Zhao D, Guan Y. Characterizing modal exponential growth behaviors of self-excited transverse and longitudinal thermoacoustic instabilities. Physics of Fluids 2022;34(2): 024109.

[7] Zhao X, Chen Y, Chen L, Chen N, Wang H, Huang W, Chen J. On full-life-cycle SOC estimation for lithium batteries by a variable structure based fractional-order extended state observer. Applied Energy 2023;351:121828.

[8] Chen Z, Zuo W, Zhou K, Li Q, Yi Z, Huang Y. Numerical investigation on the performance enhancement of PEMFC with gradient sinusoidal-wave fins in cathode channel. Energy 2024;288:129894.

[9] Chen X, Li J, Feng M, Zhao D, Shi B, Wang N. Flame stability and combustion characteristics of liquid fuel in a meso-scale burner with porous media. Fuel 2019;251:249-259.

[10] Chen J, Zhang Y, Wu J, Cheng, W, Zhu Q. SOC estimation for lithium-ion battery using the LSTM-RNN with extended input and constrained output. Energy 2023;262:125375.

[11] Han L, Li J, Zhao D, Xi Y, Gu X, Wang N. Effect analysis on energy conversion enhancement and NOx emission reduction of ammonia/hydrogen fuelled wavy micro-combustor for micro-thermophotovoltaic application. Fuel 2021289:119755.

[12] Wu L, Lyu Z, Huang Z, Zhang C, Wei C. Physics-based battery SOC estimation methods: Recent advances and future perspectives. Journal of Energy Chemistry 2024;89:27-40.

[13] Tang X, Liu K, Wang X, Liu B, Gao F, Widanage WD. Real-time aging trajectory prediction using a base model-oriented gradient-correction particle filter for Lithium-ion batteries. Journal

of Power Sources 2019;440:227118.

[14] Yang R, Xiong R, Shen W, Lin X. Extreme learning machine-based thermal model for lithium-ion batteries of electric vehicles under external short circuit. Engineering 2021;7(3):395-405.

[15] Fan X, Zhang W, Zhang C, Chen A, An F. SOC estimation of Li-ion battery using convolutional neural network with U-Net architecture. Energy 2022;256:124612.

[16] Mao X, Song S, Ding F. Optimal BP neural network algorithm for state of charge estimation of lithium-ion battery using PSO with Levy flight. Journal of Energy Storage 2022;49:104139.

[17] Guo S, Ma L. A comparative study of different deep learning algorithms for lithium-ion batteries on state-of-charge estimation. Energy 2023;263:125872

[18] Watrin N, Blunier B, Miraoui A. Review of adaptive systems for lithium batteries state-of-charge and state-of-health estimation//2012 IEEE Transportation Electrification Conference and Expo (ITEC). IEEE, 2012: 1-6.

[19] Yang N, Zhang X, Shang B, Li G. Unbalanced discharging and aging due to temperature differences among the cells in a lithium-ion battery pack with parallel combination. Journal of Power Sources 2016;306:733-741.

[20] Hannan M A, Lipu M S H, Hussain A, Mohamed A. A review of lithium-ion battery state of charge estimation and management system in electric vehicle applications: Challenges and recommendations. Renewable and Sustainable Energy Reviews 2017;78: 834-854.

[21] Feng X, Chen J, Zhang Z, Miao S, Zhu Q. State-of-charge estimation of lithium-ion battery based on clockwork recurrent neural network. Energy 2021;236:121360.

[22] Chen J, Zhang Y, Li W, Cheng W, Zhu Q. State of charge estimation for lithium-ion batteries using gated recurrent unit recurrent neural network and adaptive Kalman filter. Journal of

Energy Storage 2022;55:105396.

[23] Xing Y, He W, Pecht M, Tsui KL. State of charge estimation of lithium-ion batteries using the open-circuit voltage at various ambient temperatures. Applied Energy 2014;113:106-115.

[24] Hassan MU, Saha S, Haque ME, Islam S, Mahmud A, Mendis N. A comprehensive review of battery state of charge estimation techniques. Sustainable Energy Technologies and Assessments 2022;54:102801.

[25] Gong Q, Wang P, Cheng Z. A novel deep neural network model for estimating the state of charge of lithium-ion battery. Journal of Energy Storage 2022;54:105308.

[26] Sesidhar D, Badachi C, Green IIRC. A review on data-driven SOC estimation with Li-Ion batteries: Implementation methods & future aspirations. Journal of Energy Storage 2023;72:108420.

[27] Doyle M, Fuller TF, Newman J. Modeling of galvanostatic charge and discharge of the lithium/polymer/insertion cell. Journal of the Electrochemical society 1993;140(6):1526.

[28] Wang Q, Ye M, Wei M, Lian G, Li Y. Deep convolutional neural network based closed-loop SOC estimation for lithium-ion batteries in hierarchical scenarios. Energy 2023;263:125718.

[29] Feng F, Teng S, Liu K, Xie J, Xie Y, Liu B, Li K. Co-estimation of lithium-ion battery state of charge and state of temperature based on a hybrid electrochemical-thermal-neural-network model. Journal of Power Sources 2020;455:227935.

[30] Xile D, Caiping Z, Jiuchun J. Evaluation of SOC estimation method based on EKF/AEKF under noise interference. Energy Procedia 2018;152:520-525.

[31] He Z, Li Y, Sun Y, Zhao S, Lin C, Pan C, Wang L. State-of-charge estimation of lithium-ion batteries based on adaptive iterative extended Kalman filter. Journal of Energy Storage 2021;39:102593.

[32] Solomon OO, Zheng W, Chen J, Qiao Z. State of charge estimation of Lithium-ion battery using an improved fractional-order extended Kalman filter. Journal of Energy Storage 2022;49:104007.

[33] Zhang Y, Xiong R, He H, Shen W. Lithium-ion battery pack state of charge and state of energy estimation algorithms using a hardware-in-the-loop validation. IEEE Transactions on Power Electronics 2016;32(6):4421-4431.

[34] Mendoza S, Liu J, Mishra P, Fathy H. On the relative contributions of bias and noise to lithium-ion battery state of charge estimation errors. Journal of Energy Storage 2017;11:86-92.

[35] Shu X, Li G, Zhang Y, Shen S., Chen Z., Liu Y. Stage of charge estimation of lithium-ion battery packs based on improved cubature Kalman filter with long short-term memory model. IEEE Transactions on Transportation Electrification 2020;7(3):1271-1284.

[36] Sun H, Sun J, Zhao K, Wang L, Wang K. Data-driven ICA-Bi-LSTM-combined lithium battery SOH estimation. Mathematical Problems in Engineering 2022;2022: 9645892.

[37] Li D, Wang L, Duan C, Li Q, Wang K. Temperature prediction of lithium- ion batteries based on electrochemical impedance spectrum: a review. International Journal of Energy Research 2022;46(8):10372-10388

[38] Hu JN, Hu JJ, Lin HB, Li XP, Jiang CL, Qiu XH, Li WS. State-of-charge estimation for battery management system using optimized support vector machine for regression. Journal of Power Sources 2014;269: 682-693.

[39] Li C, Chen Z, Cui J, Wang Y, Zou F. The lithium-ion battery state-of-charge estimation using random forest regression//2014 Prognostics and System Health Management Conference (PHM-2014 Hunan). IEEE, 2014:336-339.

[40] Deng Z, Hu X, Lin X, Che Y, Xu L, Guo W. Data-driven state of charge estimation for

lithium-ion battery packs based on Gaussian process regression. Energy 2020; 205:118000.

[41] Sahinoglu GO, Pajovic M, Sahinoglu Z, Wang Y, Orlik PV, Wada T. Battery state-of-charge estimation based on regular/recurrent Gaussian process regression. IEEE Transactions on Industrial Electronics 2017;65(5):4311-4321.

[42] Chemali E, Kollmeyer PJ, Preindl M, Ahmed R, Emadi A. Long short-term memory networks for accurate state-of-charge estimation of Li-ion batteries. IEEE Transactions on Industrial Electronics 2017;65(8):6730-6739.

[43] Yang F, Li W, Li C, Miao Q. State-of-charge estimation of lithium-ion batteries based on gated recurrent neural network. Energy 2019;175:66-75.

[44] Liu Y, Li J, Zhang G, Hua B, Xiong N. State of charge estimation of lithium-ion batteries based on temporal convolutional network and transfer learning. Ieee Access 2021; 9:34177-34187.

[45] Chen J, Feng X, Jiang L, Zhu Q. State of charge estimation of lithium-ion battery using denoising autoencoder and gated recurrent unit recurrent neural network. Energy 2021;227:120451.

[46] Hu C, Cheng F, Ma L, Li B. State of charge estimation for lithium-ion batteries based on TCN-LSTM neural networks. Journal of the Electrochemical Society 2022;169(3):030544.

[47] Li N, Zhang Y, He F, Zhu L, Zhang X, Ma Y, Wang S. Review of lithium-ion battery state of charge estimation. Global Energy Interconnection 2021;4(6):619-630.

[48] Zhang K, Xiong R, Li Q, Chen C, Tian J, Shen W. A novel pseudo-open-circuit voltage modeling method for accurate state-of-charge estimation of $LiFePO_4$ batteries. Applied Energy 2023;347:121406.

[49] Xing Y, He W, Pecht M, Tsui KL. State of charge estimation of lithium-ion batteries using the open-circuit voltage at various ambient temperatures. Applied Energy 2014; 113:106-115.

[50] Liu X, Li W, Zhou A. PNGV equivalent circuit model and SOC estimation algorithm for lithium battery pack adopted in AGV vehicle. Ieee Access 2018;6:23639-23647.

[51] Ding X, Zhang D, Cheng J, Wang B, Luk P. C. K. An improved Thevenin model of lithium-ion battery with high accuracy for electric vehicles. Applied Energy 2019; 254:113615.

[52] Lin X, Tang Y, Ren J, Wei Y. State of charge estimation with the adaptive unscented Kalman filter based on an accurate equivalent circuit model. Journal of Energy Storage 2021;41:102840.

[53] Wang Y, Cheng Y, Xiong Y, Yan Q. Estimation of battery open-circuit voltage and state of charge based on dynamic matrix control-extended Kalman filter algorithm. Journal of Energy Storage 2022;52:104860.

[54] Wang L, Cheng Y, Zou J. Battery available power prediction of hybrid electric vehicle based on improved Dynamic Matrix Control algorithms. Journal of Power Sources 2014;261:337-347.

[55] Xu Z, Wang J, Fan Q, Lund P D, Hong J. Improving the state of charge estimation of reused lithium-ion batteries by abating hysteresis using machine learning technique. Journal of Energy Storage 2020;32:101678.

[56] Xiong R, Yu Q, Lin C. A novel method to obtain the open circuit voltage for the state of charge of lithium-ion batteries in electric vehicles by using H infinity filter. Applied Energy 2017;207:346-353.

[57] Sarhani M, Voß S. Chunking and cooperation in particle swarm optimization for feature selection. Annals of Mathematics and Artificial Intelligence 2022;90(7-9): 893-913.

[58] Ji B, Lu X, Sun G, Zhang W, Li J, Xiao Y. Bio-inspired feature selection: An improved binary particle swarm optimization approach. IEEE Access 2020;8:85989-86002.

[59] Lara-Benítez P, Carranza-García M, Luna-Romera JM, Riquelme JC. Temporal convolutional

networks applied to energy-related time series forecasting. Applied Sciences 2020;10(7):2322.

[60] Chen Y, Wen M, Zhang K, Yu S. Short term photovoltaic output prediction based on similar day matching and TCN attention. Electrical Measurement and Instrumentation 2020:1-9.

[61] Zhen Y, Fang J, Zhao X, Ge J, Xiao Y. Temporal convolution network based on attention mechanism for well production prediction. Journal of Petroleum Science and Engineering 2022;218:111043.

[62] He K, Zhang X, Ren S, Sun J. Deep residual learning for image recognition//Proceedings of the IEEE conference on computer vision and pattern recognition 2016: 770-778.

[63] Bai S, Kolter JZ, Koltun V. An empirical evaluation of generic convolutional and recurrent networks for sequence modeling. arXiv preprint arXiv:1803.01271, 2018.

[64] US Department of Energy. USABC Electric Vehicle Battery Test Procedures Manual;1996.

[65] Xing Y, He W, Pecht M, Tsui K L. State of charge estimation of lithium-ion batteries using the open-circuit voltage at various ambient temperatures. Applied Energy 2014;113:106-115.

[66] Dang X, Yan L, Jiang H, Wu X, Sun H. Open-circuit voltage-based state of charge estimation of lithium-ion power battery by combining controlled auto-regressive and moving average modeling with feedforward-feedback compensation method. International Journal of Electrical Power & Energy Systems 2017;90:27-36.